6G Integrated Access and Backhaul Networks with Sub-Terahertz Links

Amir Ashtari Gargari*, Matteo Pagin*, Michele Polese°, Michele Zorzi*

*Department of Information Engineering, University of Padova, Italy
email: {amirashtari, paginmatte, zorzi}@dei.unipd.it
°Institute for the Wireless Internet of Things, Northeastern University, Boston, MA
email: m.polese@northeastern.edu

***Abstract*—Integrated Access and Backhaul (IAB) is a flexible and low-cost solution to deploy ultra-dense fifth and sixth generation (5G and 6G) systems, as it enables wireless backhaul links based on the same technology and specifications as for the access links. In this paper, we consider the deployment of mixed millimeter wave (mmWave) and sub-terahertz links to increase the capacity of the backhaul network, and provide the first performance evaluation of the potential of sub-terahertz frequencies for 6G IAB. To do so, we develop a greedy algorithm that allocates frequency bands to the backhaul links (considering constraints on spectrum licenses, sharing, and congestion) and generates the wireless network mesh. We then profile the performance through a custom extension of the open-source system-level simulator Sionna that supports Release 17 IAB specifications and channel models up to 140 GHz. Our results show that IAB with sub-terahertz links can outperform a mmWave-only deployment with improvements of 4× for average user throughput and a reduction of up to 50% for median latency.**

***Index Terms*—Sub-THz Communication, IAB, Self-backhauling, Wireless Backhaul, 6G**

I. Introduction

Future wireless networks will accommodate data-rate intensive use cases which include untethered Virtual Reality (VR) and mobile metaverse applications. This will further exacerbate the congestion on mobile access networks and backhaul systems [1]. For this reason, 5th generation (5G) cellular systems have pushed into the mmWave band, with typical deployments in the spectrum around 28 GHz and 39 GHz [2], and sub-terahertz mobile links are being considered for 6th generation (6G) applications [3], [4].

Wireless networks operating at such high frequencies will be deployed with extremely high density, to improve the probability of Line-of-Sight (LOS) coverage and mitigate the impact of the harsh propagation environment. To make ultra-dense deployments viable, the 3rd Generation Partnership Project (3GPP) has standardized an extension of 5G NR, i.e., IAB, which exploits the same waveform and protocol stack to provide access to mobile users and wireless backhaul for Next Generation Node Bases (gNBs) (i.e., the IAB nodes) thus limiting the need for fiber drops. The wireless backhaul topology terminates at a gNB with fiber connectivity to the data core, the IAB donor [5]–[7]. IAB also simplifies the deployment of cellular networks in on-demand or ad hoc contexts, as it removes the need for part of the wired backhaul.

IAB networks in 5G systems are a natural application for mmWave deployments, as telecom operators can easily fit carriers with 400 MHz of bandwidth in this spectrum. In addition, the directionality that mmWave arrays introduce helps reduce the interference. Nonetheless, studies have shown that bottlenecks can emerge at IAB donors, creating congestion, high latency, and degraded Quality of Service (QoS) for the end users, especially when backhaul links are constrained to re-using the same spectrum of the access (as in in-band IAB) [8].

In this context, out-of-band IAB with sub-terahertz links is seen as a solution to support immersive multimedia data-hungry streams. Specifically, the spectrum above 100 GHz has several sub-bands that could provide bandwidths wider than 10 GHz, thus potentially data rates in the excess of tens of Gbps [9]. Backhaul—a static deployment—is a promising use case for sub-terahertz links, which need pencil-sharp beams to close the link budget and are thus less resilient to mobility compared to traditional sub-6 GHz or mmWave frequencies.

In recent years, the literature has closed several gaps in terms of circuit, antenna design [10] and physical and Medium Access Control (MAC) layer solutions for sub-terahertz systems [11]. When it comes to IAB with mixed sub-terahertz and mmWave links,[1] however, there are still several open questions in terms of network design and path selection. In this paper, we consider the problem of identifying a viable topology between IAB nodes and the IAB donors, including the carrier frequency of the backhaul links, and profile the performance that network planners can expect when mixing sub-terahertz and mmWave IAB links.

To this end, we develop a greedy path generation algorithm that automatically selects the frequency band of an IAB link

This work was partially supported by the U.S. National Science Foundation under Grant CNS-2225590 and in part by the EU MSCA ITN project MINTS "MIllimeter-wave NeTworking and Sensing for Beyond 5G" (grant no. 861222).

[1]In this paper, we consider the FR2 range of 3GPP NR (24.25 GHz to 71 GHz) as mmWaves.

(between 28 GHz and 140 GHz) and assigns routes so that each IAB node can reach the IAB donor. The frequency selection aims at avoiding bottlenecks, i.e., the algorithm selects the band that provides the highest capacity when accounting for the congestion that may arise in the proximity of the IAB donor. In addition, we consider and compare different ratios of sub-terahertz and mmWave links, which can be mapped to licensing constraints for out-of-band backhaul, and two different bandwidths for the sub-terahertz links (10 GHz and 32 GHz), which consider exclusive licensing or sharing with other services, respectively [12].

We model the IAB network in a custom-developed 3GPP Release 17 simulator based on the open-source tool Sionna [13], with 3GPP and state-of-the-art mmWave and sub-terahertz channel models, and realistic and detailed 3GPP-based physical and MAC layers. Our results quantify for the first time the performance improvement that sub-terahertz links can introduce in IAB networks, which can push beyond the limits of the in-band mmWave backhaul and support more than 50 users with 120 Mbps streams and a single donor without congestion (compared to about 33 Mbps for in-band mmWaves).

This is the first paper that provides a numerical evaluation of the potential associated with sub-terahertz links for IAB. Notably, [14] evaluates the sub-terahertz (THz) potential in backhaul networks from a physical layer perspective. This research demonstrates that sub-THz spectrum links can achieve multi-Gbps ratios in outdoor backhaul scenarios. [15] proposed unmanned aerial vehicles (UAV)-assisted backhaul solution to improve network coverage and data rate in heterogeneous networks with multiple tiers composed of sub-6 GHz, THz and UAV layers. In addition, the authors of [16] successfully adopted concurrent scheduling to increase system throughput in dense THz backhaul scheduling. Finally, [17] considers a multi-band IAB deployment, but with a bandwidth that is more limited than those considered in future 6G scenarios.

The rest of the paper is organized as follows. Sec. II introduces the system model. Sec. III describes the algorithm for frequency and path selection, which is then numerically evaluated in Sec. IV. Finally, Sec. V concludes the paper.

II. System Model

We consider a Time Division Multiple Access (TDMA) system in which a single IAB donor, featuring a fiber connectivity towards the Core Network (CN) and the Internet, exchanges data with N_{U} User Equipments (UEs). Without loss of generality, we consider uplink traffic only. To achieve uniform coverage, the donor is aided by N_{I} IAB nodes, which can be connected either to the former or to neighboring base stations, thus possibly realizing a multi-hop wireless backhaul.

We partition the time resources in T radio subframes of duration $T_{sub} = 1$ ms, and we equip all nodes with buffers. Accordingly, the data that node i transmits to gNB k during subframe t is stored in its buffer $B_k(t)$, and represents either successfully received packets, in the case of the donor, or data to be relayed to the next hop along the path during subframe $t+1$, in the case of IAB nodes.

We assume that the backhaul links operate *either in the mmWave or in the THz band* and that each IAB node features two Radio Frequency (RF) chains, which are used for the backhaul and the fronthaul communications, respectively. In both cases, gNBs are equipped with directional antennas.

When gNB $k = 0, \ldots, N_{\mathrm{I}}$, with index 0 denoting the IAB donor, receives data from node j, packets experience a Signal to Interference plus Noise Ratio (SINR) $\gamma_{s,d}$ which can be expressed as

$$\gamma_{s,d} = \frac{|h^l_{s,d}|^2 \sigma_x^2}{\sigma_n^2 + \sum_{i \in \mathcal{I}} \sigma_i^2}, \tag{1}$$

where $h^l_{s,d}$, $l \in \{mW, sT\}$ represents the equivalent channel response between the communication endpoints when using mmWave or sub-THz links, respectively. $\mathcal{I}$ denotes the set of interferers, σ_x^2, σ_i^2 and σ_n^2 are the powers of the transmitted signal, the i-th received interfering signal, and the thermal noise at the receiver, respectively.

The corresponding access (backhaul) throughput $R^{\mathrm{A}}_{j,k}(t)$ ($R^{\mathrm{B}}_{j,k}(t)$) reads

$$R^{\mathrm{A}}_{j,k}(t) = \frac{1}{T_{sub}} \sum_{l=1}^{B^t_j} \mathbb{1}\left\{\hat{b}_l(\gamma_{j,k}) = b_l\right\}, \tag{2}$$

where B^t_j denotes the number of bits transmitted from user (IAB node) j to gNB k during subframe t and $\hat{b}_l(\gamma_{j,k})$ is the l-th decoded bit at the receiver, as a function of $\gamma_{j,k}$.

Our goal is to maximize the average system sum-rate, defined as

$$\bar{R} \doteq \frac{1}{T} \sum_{j=1}^{N_{\mathrm{I}}} \sum_{t=1}^{T} R^{\mathrm{B}}_{j,0}(t), \tag{3}$$

by tuning the carrier frequency (either mmWave or THz) of each backhaul link. We remark that in this metric we take into account only the packets which are received at their final destination, i.e., the IAB donor.

A. Channel Models

mmWave channel model: For the mmWave links, we consider the 3GPP 38.901 Spatial Channel Model (SCM) [18], which models Multiple Input, Multiple Output (MIMO) wireless channels for frequencies between 0.5 and 100 GHz.

In particular, [18] outlines the procedures for generating a channel matrix $\boldsymbol{H}_{s,d}$ whose entries $h^{j,k}_{s,d}$ correspond to the impulse response of the channel between the j-th element of the antenna array of the transmitter (S), and the k-th radiating element of the antenna array of the receiver (D). Then, the channel matrix entries are combined with a frequency-flat path loss term PL.

When considering analog beamforming at both the transmitter and the receiver, the equivalent channel response $h^{mW}_{s,d}$ can be evaluated as

$$h^{mW}_{s,d} = \sqrt{10^{PL/10}} \cdot \boldsymbol{w}_d \boldsymbol{H}_{s,d} \boldsymbol{w}_s, \tag{4}$$

with $\boldsymbol{w}_s$ and $\boldsymbol{w}_d$ the beamforming vectors used at S and D, respectively.

$$\underset{\boldsymbol{P},\{\boldsymbol{S}(t)\}_t,\boldsymbol{T}}{\operatorname{argmax}} \ \bar{R}, \tag{5a}$$

$$\text{s.t. C1: } R^{\mathrm{B}}_{j,k}(t)T_{sub} \leq B_j(t) \ \ \forall\, j,\, \forall\, t \tag{5b}$$

$$\text{C2: } B_j(t+1) = \ B_j(t) + T_{sub}\left(\sum_{k=1}^{N_{\mathrm{U}}} R^{\mathrm{A}}_{k,j}(t) + \sum_{k=1}^{N_{\mathrm{I}}} R^{\mathrm{B}}_{k,j}(t) - \sum_{k=0}^{N_{\mathrm{I}}} R^{\mathrm{B}}_{j,k}(t)\right) \ \ \forall\, j,\, \forall t \tag{5c}$$

$$\text{C3: } \sum_{k=0}^{N_{\mathrm{I}}} \boldsymbol{S}\left[j,k\right](t) + \sum_{k=1}^{N_{\mathrm{I}}} \boldsymbol{S}\left[k,j\right](t) \leq 1 \ \ \forall\, j,\, \forall t \tag{5d}$$

$$\text{C4: } R^{\mathrm{B}}_{j,k}(t)\boldsymbol{S}\left[j,k\right](t) = R^{\mathrm{B}}_{j,k}(t) \ \ \forall\, j,\, \forall k,\, \forall t \tag{5e}$$

$$\text{C5: } \sum_{j,k=0}^{N_{\mathrm{I}}} \boldsymbol{T}[j,k] \leq \rho_{max} \sum_{j,k=0}^{N_{\mathrm{I}}} \boldsymbol{P}[j,k] \tag{5f}$$

THz channel model: For sub-THz, we use the physics-based channel modeling approach from [19], which includes molecular absorption and path loss. At THz-band frequencies, molecular absorption, which causes both molecular absorption loss and molecular absorption noise, is the principal factor affecting electromagnetic wave propagation. $h^{tH}_{s,d}$ is the THz-band channel model introduced in [19], with additional transmit and receive antenna gains G_S and G_D, and is given by

$$h^{tH}_{s,d}(f,d) = \frac{c}{4\pi f d}\exp\left(-\frac{k_{abs}(f)d}{2}\right)G_S G_D, \tag{6}$$

where c stands for the speed of light and k_{abs} for the medium's molecular absorption coefficient, based on the type and composition of molecules [20].

III. Sum-rate optimization via THz Link Selection

We define $\boldsymbol{P} \in \{0,1\}^{N_{\mathrm{I}}+1\times N_{\mathrm{I}}+1}$ as the matrix which represents the possible active links among gNBs, i.e., $\boldsymbol{P}[i,j] = 1$ if and only if the wireless backhaul link between gNBs i and j is a feasible link; index 0 refers to the donor. Similarly, $\boldsymbol{S}(t) \in \{0,1\}^{N_{\mathrm{I}}+1\times N_{\mathrm{I}}+1}$ and $\boldsymbol{T} \in \{0,1\}^{N_{\mathrm{I}}+1\times N_{\mathrm{I}}+1}$ represent the links which are active during subframe t, and whether they use THz spectrum or not, respectively. Our objective is to maximize the average system sum-rate, by choosing whether each link is operating in the THz or the mmWave band and the active links in each subframe. We perform the choice of $\boldsymbol{T}$ and $\boldsymbol{P}$ only once, with the goal of reducing the computational complexity of the algorithm.

The optimization problem is thus formulated as (5a). Constraint C1 ensures that nodes do not transmit more data than available in their buffer. C2 enforces the proper evolution over time of the buffers occupancy, i.e., the buffer occupancy at time t must be equal to the one in subframe $t-1$, minus (plus) the outgoing (incoming) traffic from other nodes. Constraint C3 relates to the TDMA mode of operation, and ensures that each backhaul RF chain is used at most for one transmission/reception in any given subframe, while C4 imposes that only active links can exhibit a positive rate. Finally, with C5 we set an upper bound ρ_{max} on the maximum percentage of THz links.

A. Backhaul Scheduler

We remark that due to the binary nature of the $\boldsymbol{P}, \boldsymbol{S}(t)$ and $\boldsymbol{T}$ optimization variables, (5a) is an Integer Linear Program (ILP), thus NP-hard and not solvable in polynomial time. Therefore, in this section, we present a set of algorithms that solve the path selection and configuration problem heuristically and with low complexity.

Specifically, we first describe the pre-processing steps, referred to as *distance-aware path generation* (Alg. 1) and *THz-link selection* (Alg. 2), which prune the set of possible links established among gNBs and decide which of them are to operate in the THz bands, respectively. Then, we describe the *SINR-based scheduler* (Alg. 3), which differs from the former procedures as it is executed in each subframe to track the dynamic nature of the backhaul network.

The distance-aware path generation algorithm computes the $\boldsymbol{P}$ matrix, which encodes the potential connections between IAB nodes. $\boldsymbol{P}$ reduces the system complexity by restricting possible paths from each IAB node and by avoiding loops. Specifically, Alg. 1 iterates over each IAB node n_j, establishing a connection towards the donor whenever the distance between them is smaller than d_{max}, i.e., a scenario- and frequency-dependent distance that guarantees a link performance above a certain threshold. In our case, the considered scenario involves a small and dense deployment of IAB nodes, so the path loss distance can be compensated by the antenna gain, and d_{max} for THz and mmWave are assumed to have the same value. Moreover, the proposed pre-processing step performs additional attachments between neighboring nodes, as long as the resulting link exhibits a lower length than d_{max}. The direction of such link is determined in such a way that the destination node is the closer to the donor. Even though this link may be topologically redundant, it can provide an alternative route for load balancing purposes, while still avoiding the creation of cycles.

The THz link selection policy identifies bottleneck links based on two heuristics: 1) links involving IAB nodes which are closer to the donor are more likely to be congested since

they are usually used also for relaying traffic of subtending nodes; and 2) the average buffer occupancy provides an estimate of the loads incurred on each link. Accordingly, Alg. 2 partitions the IAB nodes into disjoint sets, referred to as *tiers*. Nodes are assigned to tiers based on their distance with respect to the donor, with tier 0 indicating the closest level to the donor. Then, the various backhaul links are marked as THz in descending order with respect to the tier of the corresponding transmitting node, until the maximum ratio of non-mmWave links ρ_{max} is reached. Note that the algorithm may eventually reach a tier whose IAB nodes are not all set as THz. In this case, ties within the same tier are broken by sorting its nodes with respect to their average traffic load, which we estimate by measuring the respective buffers. That is to say, nodes with higher buffer occupancy are given priority and thus are set as THz before nodes exhibiting a lower traffic load. Note that this procedure can be based on long-term statistics, thus averaging the load of the nodes over multiple frames.

Finally, the SINR-based scheduler dynamically allocates resources, with the objective of maximizing the average sum rate by choosing a list of paths to be activated in each subframe. The rationale behind the proposed scheme is to schedule links based on their load. Specifically, in Alg. 3 we assign a transmission resource allocation priority which is directly proportional to the buffer occupancy of the transmitting node. Once the first endpoint is chosen, we determine the outgoing link by selecting the one with the highest SINR among those calculated in Alg. 1. Then, we set all links involving the corresponding transmitting and receiving nodes as infeasible (assigning zero to the corresponding transmitting (n) and receiving node (p_n^*) indices in $\boldsymbol{P}_{temp}$), and repeat the procedure by considering the remaining nodes and links only, thus ensuring that the TDMA constraint is satisfied.

IV. Performance Evaluation

This section introduces a performance evaluation based on a novel simulation setup (Sec. IV-A) in a dense cellular network (Sec. IV-B), with a comparison between different results of THz and mmWave networks (Sec. IV-C).

Algorithm 1 Distance Aware Path Generation

$d_{max} \leftarrow$ Max distance between IAB nodes of the same tier
$\boldsymbol{P} = [0]_{N_\mathrm{I}+1 \times N_\mathrm{I}+1}$
for $n_i = 1, 2, \ldots, N_\mathrm{I}$ **do**
  $d_i \leftarrow$ 3D distance between n_i and IAB donor
  if $d_i < d_{max}$ **then**
    $\boldsymbol{P}[n_i, 0] = 1$
  end if
  for $n_j = n_1 + 1, \ldots, N_\mathrm{I}$ **do**
    $d_{i,j} \leftarrow$ 3D distance between n_i and n_j
    if $d_{i,j} < d_{max}$ **then**
      $d_j \leftarrow$ 3D distance between n_j and IAB donor
      if $d_i < d_j$ **then**
        $\boldsymbol{P}[n_j, n_i] = 1$
      else
        $\boldsymbol{P}[n_i, n_j] = 1$
      end if
    end if
  end for
end for

Algorithm 2 THz Link Selection

$\boldsymbol{N}_\mathrm{T} =$ Vector of IAB nodes tier index
$\boldsymbol{N}_{sort} =$ Vector of IAB node indices, sorted with respect to their load
$\boldsymbol{T} \leftarrow [0]_{N_\mathrm{I}+1 \times N_\mathrm{I}+1}$
$d_{max} \leftarrow$ Max distance between IAB nodes of the same tier
for $n = 1, 2, \ldots, N_\mathrm{I}$ **do**
  $d \leftarrow$ 3D distance between n and IAB donor
  $\boldsymbol{N}_\mathrm{T}[n] \leftarrow \lfloor d \,/\, d_{max} \rfloor$
end for
for $i = 1, \ldots, \max(\boldsymbol{N}_\mathrm{T})$ **do**
  $\boldsymbol{N}_T^i \leftarrow \{j \mid \boldsymbol{N}_T[j] == i\}$
  $\boldsymbol{L}_i \leftarrow$ links in $\boldsymbol{P}$ where nodes of $\boldsymbol{N}_T^i$ are the transmitting node
  if $\sum_{j,k} \boldsymbol{T}[j,k] + \dim(\boldsymbol{L}_i) < \rho_{max} \sum_{j,k} \boldsymbol{P}[j,k]$ **then**
    $\boldsymbol{T}[j,k] \leftarrow 1 \; \forall \; (j,k) \in \boldsymbol{L}_i$
  else
    while $\sum_{j,k} \boldsymbol{T}[j,k] < \rho_{max} \sum_{j,k} \boldsymbol{P}[j,k]$ **do**
      $n^* \leftarrow \min_n \mid \boldsymbol{N}_{sort}[n] \cap \boldsymbol{N}_T^i \neq \emptyset$
      $(n^*, k) \leftarrow$ link $\in \boldsymbol{L}_i \mid n^*$ is the transmitting node
      $\boldsymbol{T}[n^*, k] \leftarrow 1$; $\boldsymbol{L}_i \leftarrow \boldsymbol{L}_i \setminus (n^*, k)$
    end while
  end if
end for

Algorithm 3 SINR-based Scheduler

$\boldsymbol{N}_{sort} =$ Vector of IAB nodes, sorted with respect to their load
$\boldsymbol{P}_{temp} = \boldsymbol{P}$
$\boldsymbol{S}(t) \leftarrow [0]_{N_\mathrm{I}+1 \times N_\mathrm{I}+1}$
for n in $\boldsymbol{N}_{sort}$ **do**
  $\gamma_{max} \leftarrow -\infty$
  for i in $0, \ldots, N_\mathrm{I}$ **do**
    if $\gamma_{n,i} > \gamma_{max}$ **then**
      $\gamma_{max} \leftarrow \gamma_{n,i}$
      $p_n^* \leftarrow i$
    end if
  end for
  $\boldsymbol{S}(t)[n, p_n^*] \leftarrow 1$
  $\boldsymbol{P}_{temp}[:, n], [n, :] \leftarrow [0]$; $\boldsymbol{P}_{temp}[:, p_n^*], [p_n^*, :] \leftarrow [0]$
end for

A. Simulation Setup

We have developed a system-level simulator that runs on top of Sionna [13], an open-source TensorFlow-based GPU-accelerated toolbox, and that includes the IAB networks described in Rel. 17. The proposed simulator, which is written in Python, is a system-level simulator which features 3GPP-compliant channel modeling and lower layers of the protocol stack. However, it lacks the implementation of 5G NR higher layers. Therefore, we added system-level functions like MAC-level scheduling and RLC-level buffering [21]. In addition, in this research we use the Terasim channel simulator [20] to generate channel responses and integrate them into Sionna. To accomplish this, we generate traces for each IAB node's channel response and load them into Sionna. Terasim channel model integration allows us to generate channels up to 10 THz; in this simulation campaign, the sub-THz carrier frequency is 140 GHz. Several system-level Key Performance

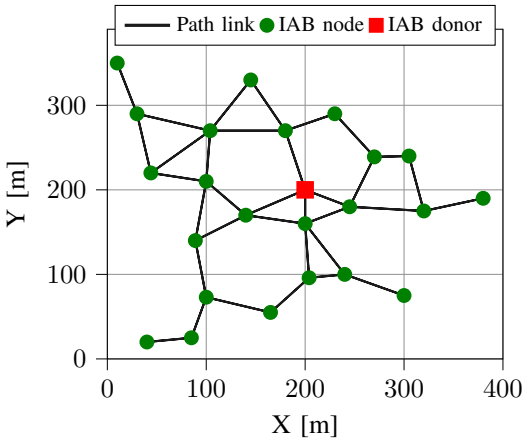

Fig. 1: Simulation Scenario

TABLE I: Simulation parameters.

Parameter	Value
Carrier frequency (mmWave)	28 GHz
Bandwidth (mmWave)	400 MHz
Carrier frequency (THz)	140 GHz
Bandwidth (THz)	$\{10, 32\}$ GHz
IAB RF Chains	2 (1 access + 1 backhaul)
Pathloss model (mmWave)	UMi-Street Canyon [18]
Pathloss model (THz)	Physics-based [19]
Number of IAB nodes N_{I}	23
Number of users N_{U}	50
Per-UE source rate	$\{40, 80, 100, 200\}$ Mbps
ρ_{max}	$\{0, 0.1, 0.3, 0.5, 0.7, 1\}$
gNB antenna array	8H $\times$ 8V
UE antenna array	4H $\times$ 4V
gNB and UE height	15 m and 1.5 m
gNB antenna gain (mmWave)	30 dB
gNB antenna gain (THz)	38 dB
Noise power	10 dBm

Indicators (KPIs), including latency, throughput, and packet loss rate, are produced by our simulator.

B. Simulation Scenario

We take a dense cellular base station deployment into account in our models. As shown in Fig. 1, we place IAB nodes at a density of 150 gNB/km^2, thus with an average intersite distance of 40 m. In Table I, the specific simulation settings are displayed. For mmWave, we used the channel model outlined by 3GPP in TR 38.901 [18], a statistical 3GPP channel model for 0.5-100 GHz, while for sub-THz we used the THz-band channel model introduced in [19] and detailed in Sec. II-A. The range of the user rate is 20 Mbps to 500 Mbps. We used a phased array antenna for mmWave and a horn antenna for THz, respectively. In mmWave we do beamforming based on a pre-generated codebook, in order to find the best beam pair for connection. For the purposes of SINR calculation, we assume that each interfering device utilizes the beamforming vector with the greatest SINR towards its intended target. In a similar fashion, both the transmitter and the receiver utilize the beamforming configuration calculated by the hierarchical search technique. We consider a scenario with a single donor to focus on the issues related to the bottleneck in the air interface of the donor itself, while extension to multiple donors is left for future work. We also set $d_{max} = 70$ m, as it has been experimentally shown that sub-THz links can operate in this range also in adverse weather conditions [22].

C. Results

In this section we report the outcomes of our numerical evaluation, focusing on end-to-end metrics measured at the IAB donor. We compare the performance achieved by different backhaul configurations, i.e., different maximum ratios of THz links and bandwidth, in terms of throughput, latency and packet drop ratio. We consider two baselines: *Random Scheduler (RS)* and *Random Links (RL)*. The former uses Alg. 2 and chooses at random a feasible set of active links during each subframe. On the contrary, RL randomly picks which links to set as THz, and uses Alg. 3 for scheduling.

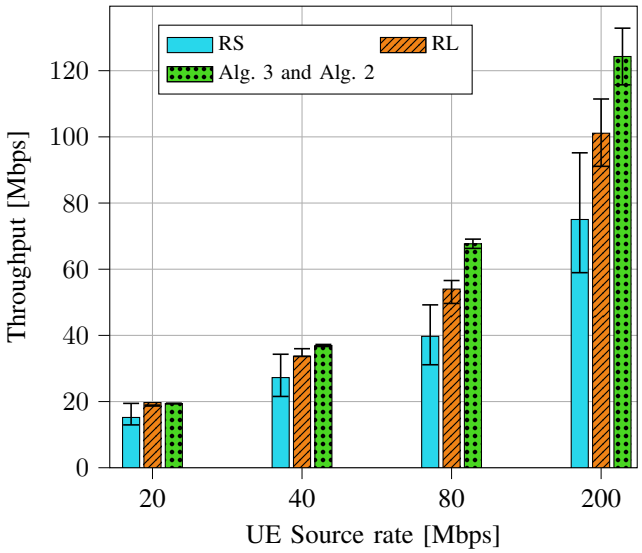

Fig. 2: Throughput per UE for different schedulers and THz link selection policies, for THz bandwidth 32 GHz and $\rho_{max} = 0.3$.

10 simulations per configuration are executed, to obtain estimates which are averaged over the realizations of the wireless channels.

Fig. 2 reports the UE throughput achieved by the proposed solution, versus that achieved by RS and RL. Focusing on the former, it can be seen that Alg. 3 leads to a throughput increase of up to 40% compared to a random scheduling policy, thanks to the prioritization of the backhaul links incurring a higher load and exhibiting a higher number of subtending IAB nodes. Moreover, Alg. 2 introduces an additional throughput increase of up to 15% compared to RL.

Fig. 3 illustrates the UE throughput for various configurations of sub-THz backhauling links and different UE source rates. The performance always improves by adding more bandwidth to the system through sub-THz links, despite the harsher propagation environment at higher frequencies. The performance gap increases with the user source rate. Indeed,

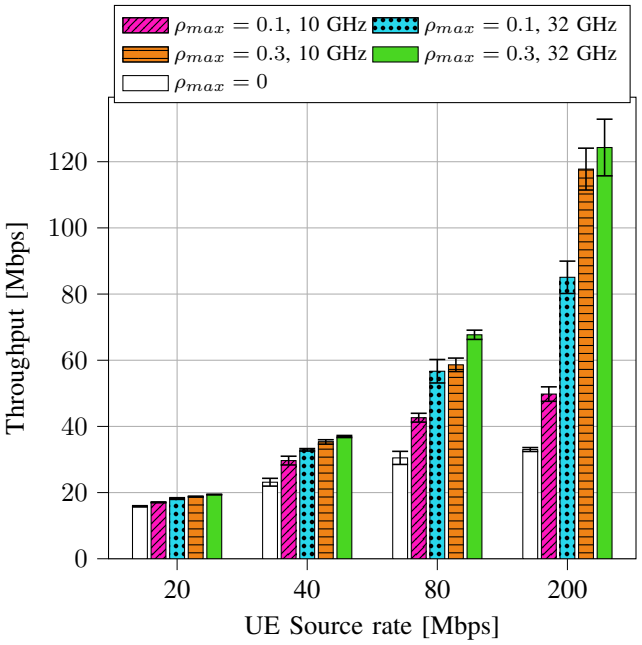

Fig. 3: Throughput per UE for different configurations.

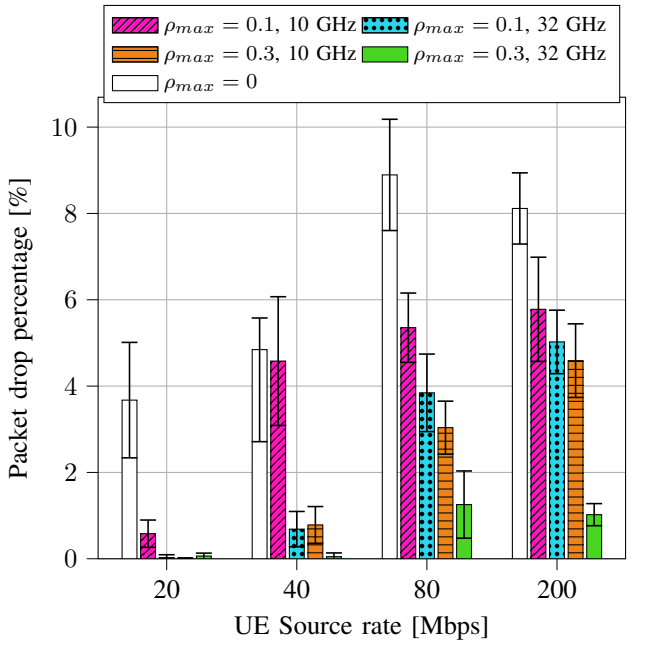

Fig. 4: Backhaul packet drop percentage for different configurations.

mmWaves successfully sustain a source system rate of 1 Gbps (20 Mbps for 50 UE), but cannot match higher source rates, as the capacity saturates. The configuration with sub-THz links achieves a higher throughput in all scenarios and in particular for $\rho_{max} = 0.3$, 32 GHz achieves the highest throughput for all source rates. It is obvious that increasing the bandwidth improves the performance; nevertheless, increasing the percentage of the THz links from $\rho_{max} = 0.1$ to $\rho_{max} = 0.3$ has a more significant impact on throughput. This may be explained by considering the effects of replacing bottleneck backhauling mmWave links with THz links with higher bandwidth.

Similar considerations can be drawn from the results shown in Fig. 4, which reports the packet drop percentages for various backhaul configurations. The highest and lowest packet drop percentages across all UE source rates are achieved when using the mmWave and $\rho_{max} = 0.3$, 32 GHz configurations, respectively. Packet drop percentages at 20 Mbps source rates are close to zero for all configurations. The highest packet drop percentages among configurations including THz is $\rho_{max} = 0.1$, 10 GHz. It is noteworthy that the system performance is influenced directly by both the THz bandwidth and the link ratio, as seen in Fig 3.

Fig. 5 depicts the Empirical Cumulative Distribution Function (ECDF) of the end-to-end (E2E) latency experienced by packets which reach the donor, for different bachkaul configurations. Accordingly, both latencies accumulated over the fronthaul and backhaul links are taken into account, from the time packets are generated at the UE until they eventually reach the IAB donor. The plot shows that packet latency decreases as more sub-THz links are added to the network. In accordance with the aforementioned observations (Fig. 3 and Fig. 4), $\rho_{max} = 0.3$, 32 GHz has the lowest latency, whereas

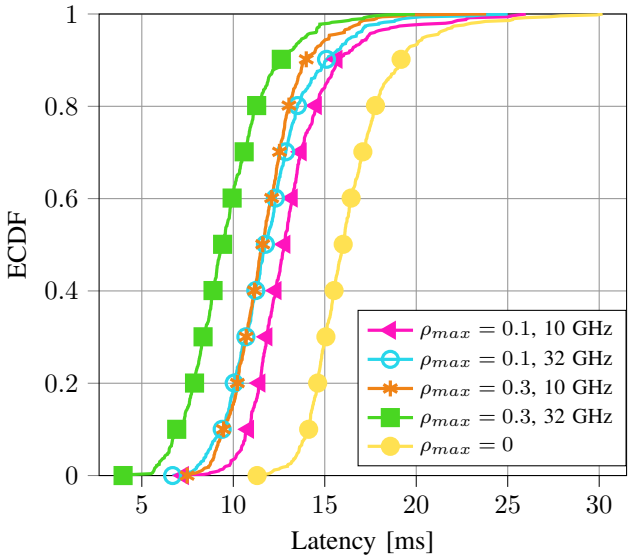

Fig. 5: E2E latency ECDF for different configurations for 80 Mbps user rate.

mmWave has the highest latency. The average latency for $\rho_{max} = 0.3$, 32 GHz, $\rho_{max} = 0.3$, 10 GHz, $\rho_{max} = 0.1$, 32 GHz, and $\rho_{max} = 0.1$, 10 GHz is approximately 51%, 24%, 24%, and 18% less than in mmWave.

Finally, the average system throughput for different ratios ρ_{max} of THz link is shown in Fig. 6. The system throughput increases with the inclusion of additional THz links. The figure also shows that system source rates of 2 Gbps, 4 Gbps, and 10 Gbps can be satisfied by a single donor when ρ_{max} is properly set. However, the larger demand of the 25 Gbps system source rate still cannot be satisfied, as the system becomes saturated. $\rho_{max} = 0.1$ and 1 can increase the system

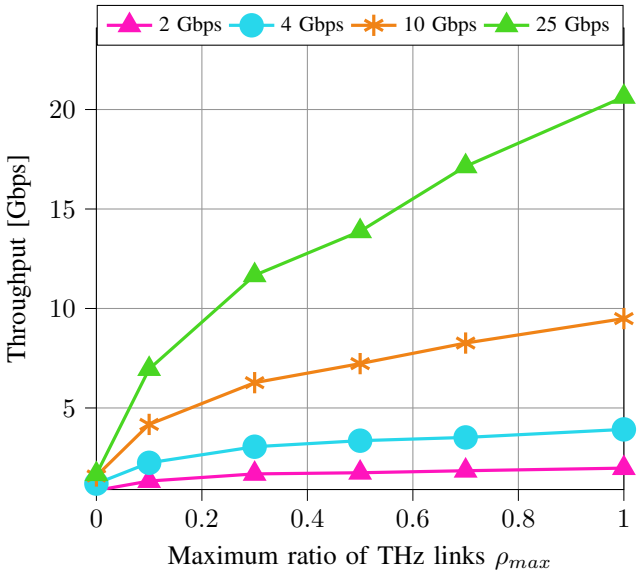

Fig. 6: System throughput for different source rate and ratio of THz links.

throughput by up to four times and twelve times, respectively.

V. Conclusions and Future Work

This paper provides the first performance evaluation of the possibilities of sub-terahertz frequencies for 6G IAB using a customized extension of the open-source Sionna simulator. This permits the use of greedy algorithms to evaluate the deployment of mixed mmWave and sub-terahertz links to boost the backhaul network's capacity. We will broaden the analysis of the network performance to cover a broader range of source traffic patterns, scenarios (including multi-donor instances, deployments with lower node density, or more realistic map-based scenarios as in [23], [24]), and protocol stack implementations as future work.

References

[1] X. Xu, Y. Pan, P. P. M. Y. Lwin, and X. Liang, "3D holographic display and its data transmission requirement," in *International Conference on Information Photonics and Optical Communications*, 2011, pp. 1–4.

[2] M. Shafi, A. F. Molisch, P. J. Smith, P. Z. T. Haustein, P. D. Silva, F. Tufvesson, A. Benjebbour, and G. Wunder, "5G: A Tutorial Overview of Standards, Trials, Challenges, Deployment, and Practice," *IEEE J. Sel. Areas Commun.*, vol. 35, no. 6, pp. 1201–1221, June 2017.

[3] M. Polese, J. M. Jornet, T. Melodia, and M. Zorzi, "Toward End-to-End, Full-Stack 6G Terahertz Networks," *IEEE Commun. Mag.*, vol. 58, no. 11, pp. 48–54, November 2020.

[4] W. Saad, M. Bennis, and M. Chen, "A Vision of 6G Wireless Systems: Applications, Trends, Technologies, and Open Research Problems," *IEEE Network*, vol. 34, no. 3, pp. 134–142, May 2020.

[5] C. Madapatha, B. Makki, C. Fang, O. Teyeb, E. Dahlman, M.-S. Alouini, and T. Svensson, "On integrated access and backhaul networks: Current status and potentials," *IEEE Open Journal of the Communications Society*, vol. 1, pp. 1374–1389, Sep. 2020.

[6] C. Saha and H. S. Dhillon, "Millimeter Wave Integrated Access and Backhaul in 5G: Performance Analysis and Design Insights," *IEEE J. Sel. Areas Commun.*, vol. 37, no. 12, pp. 2669–2684, Dec. 2019.

[7] 3GPP, "NR; Integrated Access and Backhaul (IAB) radio transmission and reception," Technical Specification (TS) 38.174, Jun. 2020, v0.1.0.

[8] M. Polese, M. Giordani, T. Zugno, A. Roy, S. Goyal, D. Castor, and M. Zorzi, "Integrated Access and Backhaul in 5G mmWave Networks: Potential and Challenges," *IEEE Commun. Mag.*, vol. 58, no. 3, pp. 62–68, Mar. 2020.

[9] I. F. Akyildiz, J. M. Jornet, and C. Han, "Terahertz band: Next frontier for wireless communications," *Physical Communication*, vol. 12, pp. 16–32, September 2014.

[10] A. Singh, M. Andrello, N. Thawdar, and J. M. Jornet, "Design and operation of a graphene-based plasmonic nano-antenna array for communication in the terahertz band," *IEEE J. Sel. Areas Commun.*, vol. 38, no. 9, pp. 2104–2117, Sep. 2020.

[11] S. Ghafoor, N. Boujnah, M. H. Rehmani, and A. Davy, "MAC Protocols for Terahertz Communication: A Comprehensive Survey," *IEEE Commun. Surveys Tuts.*, vol. 22, no. 4, pp. 2236–2282, Fourth Quarter 2020.

[12] M. Polese, V. Ariyarathna, P. Sen, J. V. Siles, F. Restuccia, T. Melodia, and J. M. Jornet, "Dynamic spectrum sharing between active and passive users above 100 GHz," *Communications Engineering*, vol. 1, no. 1, pp. 1–9, 2022.

[13] J. Hoydis, S. Cammerer, F. A. Aoudia, A. Vem, N. Binder, G. Marcus, and A. Keller, "Sionna: An open-source library for next-generation physical layer research," *arXiv preprint arXiv:2203.11854*, 2022.

[14] G. Gougeon, Y. Corre, M. Z. Aslam, S. Bicaïs, and J.-B. Doré, "Assessment of sub-THz mesh backhaul capabilities from realistic modelling at the PHY layer," in *14th European Conference on Antennas and Propagation (EuCAP)*, 2020, pp. 1–5.

[15] A. A. Raja, M. A. Jamshed, H. Pervaiz, and S. A. Hassan, "Performance analysis of UAV-assisted backhaul solutions in THz enabled hybrid heterogeneous network," in *Conference on Computer Communications Workshops (INFOCOM WKSHPS)*, 2020, pp. 628–633.

[16] H. Jiang, Y. Niu, B. Ai, Z. Zhong, and S. Mao, "QoS-aware bandwidth allocation and concurrent scheduling for terahertz wireless backhaul networks," *IEEE Access*, vol. 8, pp. 125 814–125 825, July 2020.

[17] C. Saha, M. Afshang, and H. S. Dhillon, "Integrated mmWave Access and Backhaul in 5G: Bandwidth Partitioning and Downlink Analysis," in *IEEE International Conference on Communications (ICC)*, May 2018, pp. 1–6.

[18] 3GPP, "Study on channel model for frequencies from 0.5 to 100 GHz," 3rd Generation Partnership Project (3GPP), Technical Report (TR) 38.901, Jan. 2020, version 16.1.0.

[19] J. M. Jornet and I. F. Akyildiz, "Channel modeling and capacity analysis for electromagnetic wireless nanonetworks in the terahertz band," *IEEE Trans. Wireless Commun.*, vol. 10, no. 10, pp. 3211–3221, August 2011.

[20] Z. Hossain, Q. Xia, and J. M. Jornet, "Terasim: An ns-3 extension to simulate Terahertz-band communication networks," *Nano Communication Networks*, vol. 17, pp. 36–44, September 2018.

[21] A. Ashtari Gargari, A. Ortiz, M. Pagin, A. Klein, M. Hollick, M. Zorzi, and A. Asadi, "Safehaul: Risk-Averse Learning for Reliable mmWave Self-Backhauling in 6G Networks," in *IEEE Conference on Computer Communications (INFOCOM)*, New York, USA, 2023.

[22] P. Sen, J. Hall, M. Polese, V. Petrov, D. Bodet, F. Restuccia, T. Melodia, and J. M. Jornet, "Terahertz Communications Can Work in Rain and Snow: Impact of Adverse Weather Conditions on Channels at 140 GHz," in *Proceedings of the 6th ACM Workshop on Millimeter-Wave and Terahertz Networks and Sensing Systems*, ser. mmNets '22. New York, NY, USA: Association for Computing Machinery, 2022, p. 13–18.

[23] G. Gemmi, R. L. Cigno, and L. Maccari, "On the Properties of Next Generation Wireless Backhaul," *IEEE Transactions on Network Science and Engineering*, vol. 10, no. 1, pp. 166–177, Jan 2023.

[24] G. Gemmi, R. Lo Cigno, and L. Maccari, "On Cost-Effective, Reliable Coverage for LoS Communications in Urban Areas," *IEEE Transactions on Network and Service Management*, vol. 19, no. 3, pp. 2767–2779, Sep. 2022.